

Machine Learning Reconstruction of High-Dimensional Electronic Structure from Angle-Resolved Photoemission Spectroscopy

Yu Zhang¹, Yong Zhong^{2,3*}, Nhat Huy Tran¹, Shuyi Li¹, Kyuho Lee^{3,4},
Yonghun Lee^{2,3}, Tiffany C. Wang^{2,3}, Harold Y. Hwang^{2,3}, Zhi-Xun Shen^{2,3,4},
Chunjing Jia^{1*}

¹Department of Physics, University of Florida, Gainesville, FL 32611, United States.

²Department of Applied Physics, Stanford University, Stanford, CA 94305, United States.

³Stanford Institute for Materials and Energy Sciences, SLAC National Accelerator Laboratory, Menlo Park, CA 94025, United States.

⁴Department of Physics, Stanford University, Stanford, CA 94305, United States.

*Corresponding author(s). E-mail(s): ylzhong@stanford.edu; chunjing@phys.ufl.edu;

Abstract

The emergent behavior of quantum materials is governed by their electronic structure, which can be experimentally probed by photoemission spectroscopy techniques that generate a four-dimensional dataset of energy and momentum. However, the quantitative extraction of Hamiltonian parameters from these high-dimensional spectra remains a significant challenge, currently relying on labor-intensive, expert-dependent analysis rather than standardized workflows. Here, we introduce a deep learning framework based on implicit neural representations to accelerate the retrieval of Hamiltonian parameters in two types of transition-metal oxides: perovskite nickelates and manganites. Our approach outperforms traditional analytical fitting procedures, yielding superior agreement with experimental Fermi surface topologies and energy-momentum dispersions. This work highlights the potential of deep learning tools to bridge the gap between theory and experiment, paving the way for high-throughput, autonomous discovery pipelines in quantum materials.

Introduction

Artificial Intelligence (AI) has catalyzed a paradigm shift in the natural sciences, most dramatically in biology, where deep learning architectures such as AlphaFold have solved long-standing challenges in protein structure prediction and gene sequence analysis [1, 2]. This breakthrough provides a compelling blueprint for the next frontier in materials science: the AI-driven discovery of quantum materials. By leveraging deep learning tools to decode materials’ “genome” — the underlying electronic structures, novel quantum states can be rationally designed to meet the demands of high-temperature superconductivity, exotic magnetism and non-trivial topology.

Modern AI techniques have emerged as a transformative force in the theoretical prediction of electronic structures. At the density functional theory (DFT) level, recent developments include efficient mapping of potential energy surfaces via DeepMD [3, 4] and general machine learning interatomic potentials (MLIPs) such as EquiformerV2 and MatterSim [5, 6], as well as direct prediction of electronic band dispersions using frameworks like DeepH [7, 8]. These pioneering approaches learn from large datasets of first-principles DFT or *ab initio* molecular dynamics calculations, enabling the simulation for greatly more complex systems with remarkable efficiency. Beyond interatomic potentials, neural-network quantum states (NQS) provide a powerful route to solving strongly correlated systems based on model Hamiltonians. By employing restricted Boltzmann machine (RBM) [9] and Transformers-based [10, 11] architectures, open-source tools such as NetKet [12] and DeepSolid [13] capture strong electronic correlations and entanglement effects beyond the mean-field level. Recent developments have extended these capabilities to spectral functions [14–16], enabling investigation of both static and dynamical electronic properties.

Although rapid advances have been achieved in the theoretical frontier of electronic structure prediction, the ability to benchmark these results with experimental observations remains a critical bottleneck. Angle-resolved photoemission spectroscopy (ARPES) is the most direct experimental technique for probing the electronic structure of quantum materials [17]. By resolving both energy (E) and momentum (\mathbf{k}), it generates a four-dimensional dataset (E, k_x, k_y, k_z) that encapsulates the full electronic information. Despite these unparalleled capabilities, high-quality ARPES datasets are severely limited by practical barriers: experiments require access to large-scale synchrotron facilities and involve low-throughput acquisition cycles spanning tens of hours. Moreover, downstream analysis is labor-intensive and contingent upon expert bias. Therefore, the development of dedicated AI frameworks is essential to accelerate the analysis of high-dimensional spectral data.

Deep learning has demonstrated increasingly important utilities across diverse spectroscopic techniques. It has been widely used to uncover crucial material properties through feature extraction [18–20], high-fidelity denoising [21] and spectral prediction [22]. Within the specific domain of ARPES, nascent efforts have employed deep learning architectures to address specialized problems, such as probabilistic band retrieval [23], superconducting gap determination [24], and multidimensional data cleaning [25]. Despite these localized successes, a generalized AI framework capable of directly extracting fundamental electronic parameters from raw ARPES data remains elusive. This objective is hindered by several challenges: the scarcity of standardized experimental repositories, the intrinsic complexity of many-body electronic interactions, and the experimental noise inherent to the measurement process.

In this work, we address this critical gap by providing a first-of-its-kind approach to capturing fundamental electronic Hamiltonian parameters directly from experimental ARPES data. We incorporate a physics model to guide a machine learning (ML) architecture in learning the underlying physics. We use two real-world examples, perovskite nickelate and manganite, to demonstrate the power of deep learning methods for ARPES data interpretation. The algorithm delivers reconstructions that agree excellently with experimental spectra for both materials, demonstrating that an ML-based approach can automatically extract high-dimensional electronic parameters with markedly greater clarity, computational efficiency, and transferability than conventional techniques.

Results

The perovskite nickelate $\text{Nd}_{1-x}\text{Sr}_x\text{NiO}_3$ is a promising candidate for next-generation electronic devices, characterized by a sharp, tunable metal-insulator transition [26–30]. Its low-energy electronic structure is primarily governed by the two e_g orbitals of the Ni^{3+} ion, as shown in Figure 1a. Recently, systematic ARPES measurements have succeeded in mapping the high-quality, four-dimensional electronic structure of $\text{Nd}_{1-x}\text{Sr}_x\text{NiO}_3$ with $x = 0.175$ [31]. This rich experimental dataset makes perovskite nickelate an ideal model system for developing ML tools to automatically extract the essential electronic parameters underpinning its unique properties.

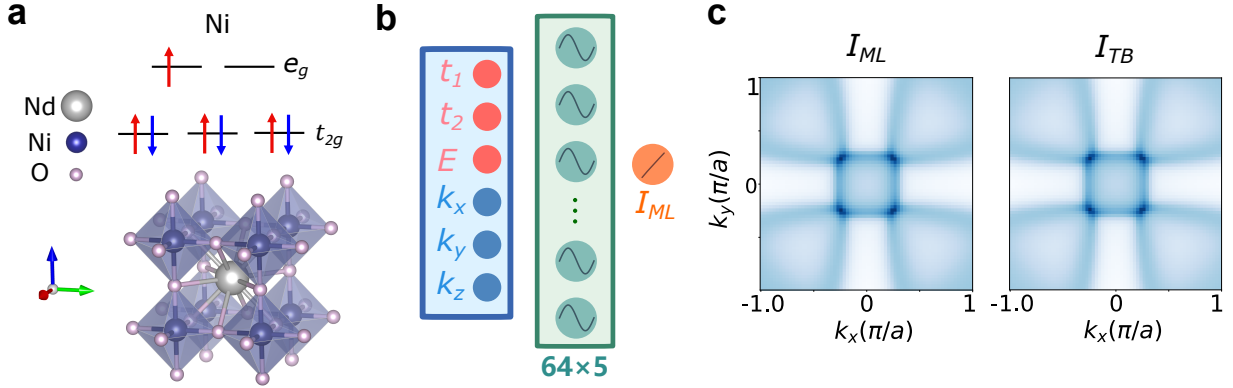


Fig. 1: **a.** Crystal structure of $\text{Nd}_{1-x}\text{Sr}_x\text{NiO}_3$ with the corresponding electronic configuration of Ni^{3+} . **b.** Architecture of the SIREN model: five hidden layers are placed between the inputs (three tight-binding parameters and \mathbf{k}) and the output (spectral intensity I_{ML}). **c.** Fermi surface obtained from the trained machine learning model (left) and from the tight-binding model (right).

Two-Band Tight-Binding Model

To capture the essential low-energy physics of perovskite nickelate, we employ a tight-binding model to simulate its electronic structure. This model is designed to reproduce two critical features in the ARPES study: band dispersion and Fermi surface topology. The band dispersion, $E(\mathbf{k})$, describes the relationship between the energy of an electron and its momentum. The Fermi surface—the boundary in momentum space separating occupied from unoccupied states—dictates many of the key properties of the material. Based on the electronic configuration of Ni^{3+} ion, a two-band tight-binding Hamiltonian can provide an effective description of the band dispersion and the Fermi surface topology for $\text{Nd}_{1-x}\text{Sr}_x\text{NiO}_3$ system [32]:

$$H_{tb} = - \sum_{ij} t_{ij}^{ab} c_{ia}^\dagger c_{jb} - \mu \quad (1)$$

Here, i, j are site indices, $a, b = 1, 2$ are orbital indices corresponding to $d_{3z^2-r^2}$ and $d_{x^2-y^2}$ orbitals, and μ is the chemical potential which can be tuned by changing the doping levels. Only the nearest-neighbor hopping t_1 and next-nearest-neighbor hopping t_2 with σ -type bonding are considered in our simulations.

We can calculate ARPES spectral intensity $I_{TB}(E, \mathbf{k})$ through equations (2) and (3), where $\epsilon(\mathbf{k})$ represents the bare band, $\Sigma'(E)$ and $\Sigma''(E)$ are the real and imaginary parts of self-energy, respectively, and $f(E)$ is the Fermi-Dirac function. The k_z broadening is taken into account by applying a Lorentzian convolution with $\Delta k_z = 0.2\frac{\pi}{a}$. The resulting spectral intensity varies with different choices of (t_1, t_2, μ) .

$$A(E, \mathbf{k}) = \sum - \frac{1}{\pi} \frac{\Sigma''(E)}{(E - \epsilon(\mathbf{k}) - \Sigma'(E))^2 + (\Sigma''(E))^2} \quad (2)$$

$$I_{TB}(E, k_x, k_y) = \int_{k_z^0 - \frac{\Delta k_z}{2}}^{k_z^0 + \frac{\Delta k_z}{2}} f(E) \frac{A(E, \mathbf{k})}{(k_z - k_z^0)^2 + (\Delta k_z/2)^2} \quad (3)$$

Implicit Neural Representations

Conventional analytical approaches for extracting electronic parameters from ARPES data are often hindered by complex dependence on model parameters, the vast momentum-energy configurational space, and the presence of experimental noise. To address these challenges, we developed a ML framework that utilizes implicit neural representations to navigate the tight-binding parameter space. Our method, inspired by the work of Chitturi et al. [33] for neutron spectroscopy analysis, provides a robust and high-fidelity alternative for parameter extraction. Specially, our model aims to obtain the tight-binding parameters (t_1, t_2, μ) that best fit the experimental ARPES spectra.

To simulate the tight-binding model for different parameters, we implement a fully connected neural network with sinusoidal activation functions, specifically the sinusoidal implicit neural representation (SIREN) model, as shown in Figure 1b. SIREN model can capture fine details for natural signals [34]. Considering the intrinsic three-dimensional electronic structure of $\text{Nd}_{1-x}\text{Sr}_x\text{NiO}_3$, we chose $(k_x, k_y, k_z, t_1, t_2, \mu)$ as inputs,

and the ML model is trained to approximate the ARPES intensity $I_{ML}(E, \mathbf{k})$. While discrete data points are used for training, the ML model is capable of interpolation to provide a continuous representation.

Based on the well-trained and differentiable neural network, we optimize the unknown tight-binding parameters using a gradient-based optimization algorithm. More specifically, we use the Pearson correlation coefficient r :

$$r = \frac{Cov(y, y_{pred})}{\sigma_y \sigma_{y_{pred}}} \quad (4)$$

as a metric to assess the similarity between I_{ML} and I_{TB} (Figure 1c). We assume that these two values are linearly correlated. Since r is invariant under linear transformation, we can avoid the normalization problem in this case. We define the loss function as $L = 1 - r$, using the SIREN model as the surrogate for the tight-binding model. We minimize L via Adam optimizer[35], following the workflow as shown in Figure 2a.

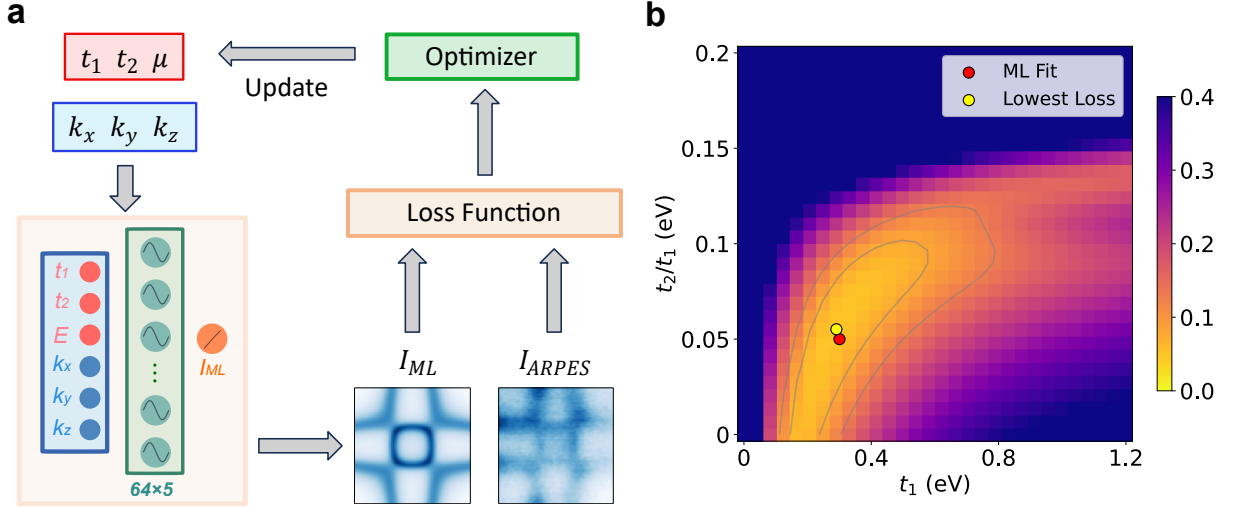


Fig. 2: **a.** Our machine learning workflow to obtain the materials parameters. An initial guess of the tight-binding parameters is fed into the well-trained SIREN model. The parameters are iteratively updated using the gradient $\frac{\partial L}{\partial t_i}$ until convergence. **b.** Visualization of the loss landscape at $\mu = 1.9t_1$. A grid of 30 sampled values was employed for both t_1 and t_2 . The color map represents the loss calculated by the trained ML model for the corresponding tight-binding parameters. Red and yellow points indicate the results from the ML fitting method and grid search (30×30), respectively.

Figure 2b shows that the tight-binding parameters, nearest neighbor hopping t_1 and the ratio of next-nearest-neighbor to nearest-neighbor hopping t_2/t_1 , obtained from the gradient optimization method lie close to the global minimum of the loss landscape at fixed chemical potential $\mu = 1.9t_1$, providing a reliable approximation. The small discrepancies between the ML obtained parameters and the global minimum can be attributed to two factors: (1) the discrete grid search, which may not capture the exact minimum due to limited resolution, and (2) the trained ML model not perfectly matching the tight-binding model, leading to minor variations.

Comparison with experimental results

To evaluate the performance of our method, we present a comprehensive comparison of the experimental data and the ML simulations in Figure 3. The first five columns show the Fermi surfaces, while the last two present the $E(\mathbf{k})$ dispersions. By comparing with the traditionally analytical fittings [31], we find that a clear improvement is achieved in the Fermi surface topology generated using the ML-optimized parameters, which exhibits a better agreement with the experimental data. This is particularly evident near the (π, π) region at photon energies of 150 eV and 155 eV. We want to emphasize that our simulation does not include matrix element effects, which can account for the intensity differences observed at symmetric \mathbf{k} -points in the experimental data. Regarding the $E(\mathbf{k})$ dispersion, the ML method also gives a better description of the “waterfall” feature extending to deep energies, which originates from many-body correlation effects [36, 37].

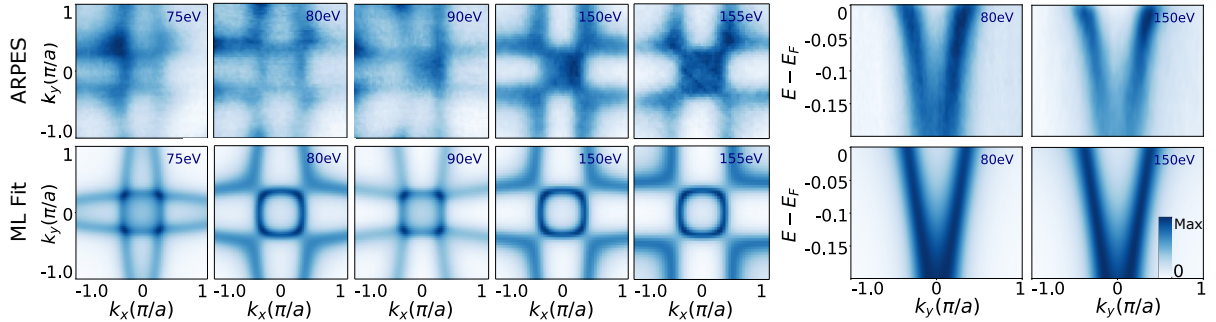


Fig. 3: Fermi surface and E_k dispersion for perovskite nickelates. Comparison between ARPES data (1st Row) and ML predictions (2nd Row) uses ML-fitted parameters with $t_1 = 0.31\text{eV}$, $t_2/t_1 = 0.05$, $\mu/t_1 = 1.94$. The blue values on each graph represent the photon energy used during measurement.

Generalization to perovskite manganite

More importantly, once the ML surrogate is well trained, the proposed framework can be easily generalized to other materials that share the same underlying tight-binding model. To demonstrate this generalization, we applied our approach to the manganite system $\text{La}_{1-x}\text{Sr}_x\text{MnO}_3$ with $x = 0.33$ [38]. As illustrated in Figure 4b and c, our approach extracts tight binding parameters without requiring any prior knowledge. Notably, the entire process is completed within five minutes. The ML-predicted Fermi surfaces across various photon energies reproduce the ARPES results quite well, offering significantly enhanced resolution to uncover the underlying physics of this material. The loss landscape in Figure 4c shows that the ML procedure achieves a minimal loss nearly coinciding with the global minimum, indicating that the predicted parameters ($t_1 = 0.42\text{eV}$, $t_2/t_1 = 0.06$, and $\mu/t_1 = 1.23$) provide a globally optimal description of the combined Fermi-surface and band-dispersion data. It is worth noting that, since the predicted parameters attempt to best fit the input data, it is essential to have guidance on the reliability and consistency of the experimental datasets used for prediction.

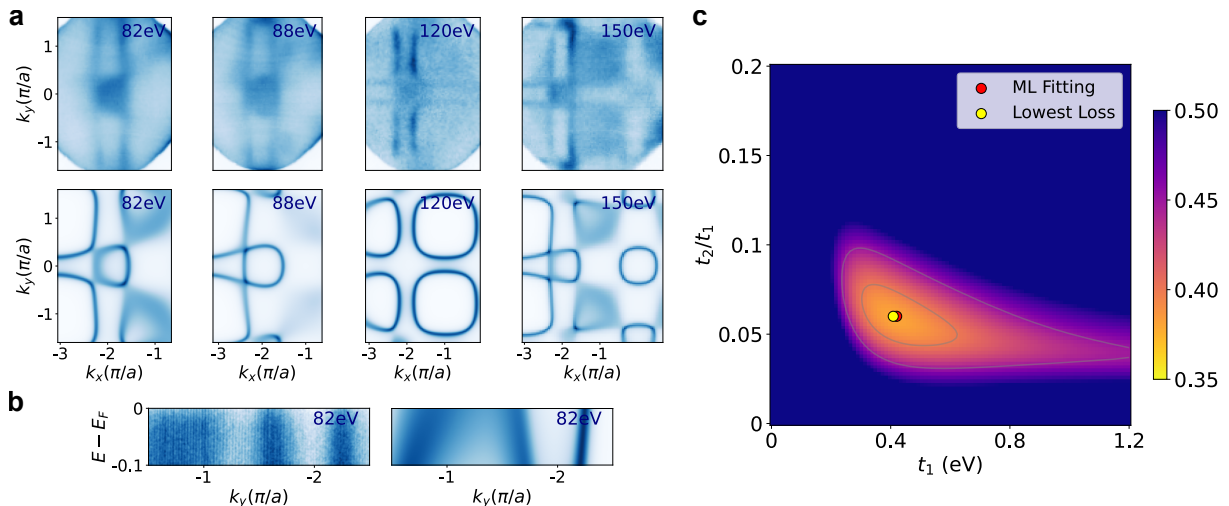


Fig. 4: **a.** $\text{La}_{1-x}\text{Sr}_x\text{MnO}_3$ ($x = 0.33$) ARPES Fermi surface measurements (top row) and ML predictions (bottom row) with parameters $t_1 = 0.42\text{eV}$, $t_2/t_1 = 0.06$, $\mu/t_1 = 1.23$. **b.** ARPES band dispersion (left panel) and ML predicted band dispersion (right panel). The blue values in the upper right corner of each panel in **a** and **b** represent the photon energy used during ARPES measurements. **c.** Visualization of the loss landscape at $\mu = 1.2t_1$ with 101×101 grid for both t_1 and t_2 . Both the Fermi surface and band dispersion ARPES data in **a** and **b** are utilized during the ML procedure.

Discussion

Our work successfully bridges the gap between the complex experimental data and the theoretical models by using a SIREN-based neural network to simulate the electronic structure of perovskite nickelates and

manganites. The quantitative agreement demonstrates that ML-driven approach can automate the reconstruction of high-dimensional ARPES data with much improved resolution. The primary advantages of this method are its efficiency, accuracy, and transferability. With an affordable initial training cost, the model can be directly applied to similar material systems without retraining. This technique offers a robust and standardized alternative to labor-intensive fitting procedures, opening a new avenue for the high-throughput analysis of electronic structures in materials science.

Looking ahead, our framework points toward a broader integration of domain-specific deep learning with emerging advances in large language models. One direction is to combine models trained on spectroscopic data with more general reasoning tools, enabling AI systems to autonomously navigate model selection — for example, determining the relevant degrees of freedom, lattice symmetries, or matrix element terms needed for accurate electronic structure reconstruction. Such an integration could evolve into agent-like platforms that not only fit data, but also reason about the appropriate physical model and adapt to new material classes with minimal human input. Ultimately, this vision suggests a path toward autonomous discovery pipelines, where spectroscopic data across diverse quantum materials are interpreted in real time, providing unprecedented scalability and consistency in connecting experiments with theory.

Methods

Sample preparation

The training data were collected from a series of $\text{Nd}_{0.825}\text{Sr}_{0.175}\text{NiO}_3$ single-crystalline thin films synthesized via pulsed-laser deposition (PLD) on LSAT(001) substrates. The generalized example of $\text{La}_{0.67}\text{Sr}_{0.33}\text{MnO}_3$ thin films were grown by the same PLD technique on STO(001) substrates.

ARPES experiments

The ARPES measurements were performed at the Stanford Synchrotron Radiation Lightsource (SSRL) beamline 5-2, equipped with a Scienta DA30 analyzer. To ensure optimal surface quality, thin films were annealed at 500 °C for 20 min under a base pressure of 1×10^{-5} Torr of purified ozone. Linear-horizontally polarized light with photon energies ranging from 60 eV to 180 eV was used to map the three-dimensional electronic structure. The base pressure during the ARPES measurements was better than 3×10^{-11} Torr. All data were acquired at a base temperature of 10 K. For $\text{Nd}_{1-x}\text{Sr}_x\text{NiO}_3$, the Fermi Surfaces were measured in the 1st Brillouin Zone (BZ) using incident photon energies of 70, 75, 80, 90, 150, 155 eV, while band dispersions along X ($k_x = 1, k_y = 0$) to M ($k_x = 1, k_y = 1$) were recorded at 80 and 150 eV. For $\text{La}_{1-x}\text{Sr}_x\text{MnO}_3$, the FS were measured at 82, 88, 120, and 150 eV, with band dispersion measured at 82 eV.

Tight-binding model

The tight-binding Hamiltonian is given by:

$$H_{tb} = - \sum_{ij} t_{ij}^{ab} c_{ia}^\dagger c_{jb} - \mu$$

The hopping parameters are defined as:

$$\begin{aligned} t_{i,i\pm\hat{\mu}}^{ab} &= t_1 \phi_\mu^a \phi_\mu^b \\ t_{i,i\pm\hat{\mu}\pm\hat{\nu}}^{ab} &= t_2 (\phi_\mu^a \phi_\nu^b + \phi_\mu^b \phi_\nu^a) \end{aligned}$$

where:

$$\phi_x = \left(-\frac{1}{2}, \frac{\sqrt{3}}{2}\right), \quad \phi_y = \left(-\frac{1}{2}, -\frac{\sqrt{3}}{2}\right), \quad \phi_z = (1, 0)$$

These correspond to the wave functions for $d_{3x^2-r^2}$, $d_{3y^2-r^2}$, and $d_{3z^2-r^2}$ σ -bonding orbitals along the three axes. We diagonalize H_{tb} to obtain the bare band dispersion for the system.

Data generation

The experimental data include both the Fermi Surface and the E(k) dispersion. Based on the data range, we synthesize ARPES intensities in selected \mathbf{k} (k_x, k_y, k_z) points, as shown in Table.1. k_x, k_y are renormalized and have units of π/a , where a is the lattice constant. k_z is computed using the following equation:

$$k_z = \sqrt{2m(\hbar\nu - \phi - E_B + V) - k_x^2 - k_y^2}/\hbar \quad (5)$$

where $h\nu$ is the incident photon energy, ϕ is the work function, E_B is the binding energy and V is the inner potential. We set $\phi = 4.4\text{eV}$, $V = 12\text{eV}$ and $\Sigma' = 0, \Sigma'' = 100\text{meV}, \Delta k_z = 0.2\frac{\pi}{a}$ for both materials. The dataset is generated using the parameters listed in Table 1, each of which is randomly and uniformly sampled from its specified range. The dataset is then divided into training, validation, and test sets in an 8:1:1 ratio.

Table 1: Summary of the parameters used to generate the synthetic ARPES data.

| Parameter | $k_x(\pi/a)$ | $k_y(\pi/a)$ | $h\nu(\text{eV})$ | $t_1(\text{eV})$ | t_2/t_1 | μ/t_1 |
|-----------|--------------|--------------|-------------------|------------------|-----------|------------|
| Range | [-3, 1] | [-1, 3] | [70, 160] | [0, 1.2] | [0, 0.2] | [0.5, 2.5] |
| Quantity | 201 | 201 | 12 | 50 | 12 | 16 |

SIREN model training

The SIREN model was trained to predict spectral intensity by minimizing the Mean Squared Error (MSE) between I_{ML} and I_{TB} . We use the Adam optimizer, batch size = 65536, initial learning rate = 0.001, which is decayed exponentially. The model was trained for 55 epochs on an NVIDIA B200 GPU. To accelerate training, only one-fifth of the training dataset was used in each epoch, resulting in an average epoch duration of approximately 150s.

Tight-binding parameters extraction

The tight-binding parameters were optimized using the Adam algorithm with an initial learning rate = 0.01 and an exponential decay for 2000 iterations. To integrate all experimental datasets, we employed a weighted loss function, where the weights were determined by the number of data points N_i in each ARPES dataset.

$$L = \frac{1}{N_{all}} \sum_i L_i N_i \quad (6)$$

In our simulation, the matrix element was not included, resulting in a symmetrized Fermi surface in the 1st Brillouin Zone (BZ). For gradient-based optimization, we used 1/4 of the ARPES Fermi surface data in 1st BZ and part of ($E - E_F > -0.1\text{eV}$) E(k) dispersion data. Table 2 and 3 summarize the experimental data used for parameter extraction, including the incident photon energy, cutting boundaries, and data size.

Table 2: Nd_{1-x}Sr_xNiO₃ data for tight-binding parameters extraction.

| Photon Energy (eV) | 75 | 80 | 90 | 150 | 155 |
|--------------------|---------|---------|--------|---------|---------|
| k_x | [-1, 0] | [-1, 0] | [0, 1] | [-1, 0] | [-1, 0] |
| k_y | [0, 1] | [0, 1] | [0, 1] | [0, 1] | [0, 1] |
| Size | 1296 | 1225 | 1122 | 625 | 600 |

| Photon Energy (eV) | 80 | 150 |
|--------------------|-----------|-----------|
| k_x | [0, 1] | [0, 1] |
| $E - E_k$ | [0, -0.1] | [0, -0.1] |
| Size | 16443 | 23616 |

Data Availability

The code used for analysis is available at <https://github.com/YuZ-TvT/ML-ARPES.git>. Data is available upon reasonable request.

Table 3: $\text{La}_{1-x}\text{Sr}_x\text{MnO}_3$ data for tight-binding parameters extraction.

| Photon Energy (eV) | 82 | 88 | 120 | 150 | Photon Energy (eV) | 82 |
|--------------------|----------|----------|------------|---------|--------------------|--------------|
| k_x | [-3, -1] | [-3, -1] | [-3, -0.5] | [-3, 0] | k_x | [-0.5, -2.5] |
| k_y | [-1, 1] | [-1, 1] | [-1, 1] | [-1, 1] | $E - E_k$ | [0, -0.1] |
| Size | 4623 | 4290 | 3864 | 3700 | Size | 45040 |

Acknowledgments

This work is supported by the U.S. Department of Energy, Office of Science, Basic Energy Sciences under Award No. DE-SC0022216. The work at SIMES and SLAC was supported by the U.S. Department of Energy, Office of Basic Energy Sciences, Division of Materials Sciences and Engineering, under contract no. DE-AC02-76SF00515. The calculations are conducted at the University of Florida Research Computing.

Author Contribution

The project was designed by C. J., Yong Z. and Z.-X. S.. Yong Z. performed the ARPES measurements. Yu Z. and Yong Z. performed the machine learning training with the help of C. J., H. T., S. L., K. L., Y. L. and T. C. W. prepared the thin films under the advice of H.H.. The manuscript was written by Yu Z., Yong Z. and C.J. with input from all coauthors.

Competing Interest

We have no conflict of interest to disclose.

References

- [1] Jumper, J., Evans, R., Pritzel, A., Green, T., Figurnov, M., Ronneberger, O., al., K.T.: Highly accurate protein structure prediction with alphafold. *Nature* **596**, 583 (2021) <https://doi.org/10.1038/s41586-021-03819-2>
- [2] Ji, Y., Zhou, Z., Liu, H., Davuluri, R.V.: Dnabert: pre-trained bidirectional encoder representations from transformers model for dna-language in genome. *Bioinformatics* **37**, 2112 (2021) <https://doi.org/10.1093/bioinformatics/btab083>
- [3] Zhang, L., Han, J., Wang, H., Car, R., E, W.: Deep potential molecular dynamics: A scalable model with the accuracy of quantum mechanics. *Physical Review Letters* **120**(14), 143001 (2018) <https://doi.org/10.1103/PhysRevLett.120.143001>
- [4] Zeng, J., Zhang, D., Lu, D., Mo, P., Li, Z., Chen, Y., Ruan, M., Yang, H., Wang, H., Zhang, L.: Deepmd-kit v2: A software package for deep potential models. *The Journal of Chemical Physics* **159**(5), 054801 (2023) <https://doi.org/10.1063/5.0155600>
- [5] Liao, Y.-L., Wood, B., Das, A., Smidt, T.: EquiformerV2: Improved Equivariant Transformer for Scaling to Higher-Degree Representations (2024)
- [6] Zuo, Y., Liu, H., Li, X., et al.: Mattersim: A deep learning atomistic model across phase space. arXiv preprint arXiv:2405.04967 (2024). Microsoft Research AI4Science
- [7] Li, H., Wang, Z., Zou, N., Ye, M., Xu, R., Gong, X., Duan, W., Xu, Y.: Deep-learning density functional theory hamiltonian for efficient ab initio electronic-structure calculation. *Nature Computational Science* **2**(6), 367–377 (2022) <https://doi.org/10.1038/s43588-022-00265-6>
- [8] Gong, X., Li, H., Zou, N., Xu, R., Duan, W., Xu, Y.: General framework for e(3)-equivariant neural network representation of density functional theory hamiltonian. *Nature Communications* **14**(1), 2848 (2023) <https://doi.org/10.1038/s41467-023-38468-8>
- [9] Carleo, G., Troyer, M.: Solving the quantum many-body problem with artificial neural networks. *Science* **355**(6325), 602–606 (2017) <https://doi.org/10.1126/science.aag2302>

- [10] Zhang, Y.-H., Di Ventura, M.: Transformer quantum state: A multipurpose model for quantum many-body problems. *Phys. Rev. B* **107**, 075147 (2023) <https://doi.org/10.1103/PhysRevB.107.075147>
- [11] Sobral, J.A., Perle, M., Scheurer, M.S.: Physics-informed transformers for electronic quantum states. *Nature Communications* **16**(1), 10811 (2025) <https://doi.org/10.1038/s41467-025-10811-y>
- [12] Vicentini, F., Hofmann, D., Szabó, A., Wu, D., Roth, C., Giuliani, C., Pescia, G., Nys, J., Vargas-Calderón, V., Astrakhantsev, N., Carleo, G.: NetKet 3: Machine learning toolbox for many-body quantum systems. *SciPost Physics Codebases*, 7 (2022) <https://doi.org/10.21468/SciPostPhysCodeb.7>
- [13] Li, X., Li, Z., Chen, J.: Ab initio calculation of real solids via neural network ansatz. *Nature Communications* **13**(1), 7891 (2022) <https://doi.org/10.1038/s41467-022-35627-1>
- [14] Mendes-Santos, T., Schmitt, M., Heyl, M.: Highly resolved spectral functions of two-dimensional systems with neural quantum states. *Phys. Rev. Lett.* **131**, 046501 (2023) <https://doi.org/10.1103/PhysRevLett.131.046501>
- [15] Yoshioka, N., Mizukami, W., Nori, F.: Solving quasiparticle band spectra of real solids using neural-network quantum states. *Communications Physics* **4**(1), 106 (2021) <https://doi.org/10.1038/s42005-021-00609-0>
- [16] Hendry, D., Chen, H., Weinberg, P., Feiguin, A.E.: Chebyshev expansion of spectral functions using restricted boltzmann machines. *Phys. Rev. B* **104**, 205130 (2021) <https://doi.org/10.1103/PhysRevB.104.205130>
- [17] Sobota, J.A., He, Y., Shen, Z.-X.: Angle-resolved photoemission studies of quantum materials. *Reviews of Modern Physics* **93**, 025006 (2021) <https://doi.org/10.1103/RevModPhys.93.025006>
- [18] Chen, Z., Andrejevic, N., Drucker, N.C., Nguyen, T., Xian, R.P., Smidt, T., Wang, Y., Ernstorfer, R., Tennant, D.A., Chan, M., Li, M.: Machine learning on neutron and x-ray scattering and spectroscopies. *Chemical Physics Reviews* **2**(3), 031301 (2021) <https://doi.org/10.1063/5.0049111>
- [19] Chitturi, S.R., Ji, Z., Petsch, A.N., Peng, C., Chen, Z., Plumley, R., Dunne, M., Mardanya, S., Chowdhury, S., Chen, H., Bansil, A., Feiguin, A., Kolesnikov, A.I., Prabhakaran, D., Hayden, S.M., Ratner, D., Jia, C., Nashed, Y., Turner, J.J.: Capturing dynamical correlations using implicit neural representations. *Nature Communications* **14**(1), 5852 (2023) <https://doi.org/10.1038/s41467-023-41378-4>
- [20] Ziatdinov, M., Ghosh, A., Wong, C.Y., Kalinin, S.V.: Atomai framework for deep learning analysis of image and spectroscopy data in electron and scanning probe microscopy. *Nature Machine Intelligence* **4**(12), 1101–1112 (2022) <https://doi.org/10.1038/s42256-022-00555-8>
- [21] Oppliger, J., Denner, M.M., Küspert, J., Frison, R., Wang, Q., Morawietz, A., Ivashko, O., Dippel, A.-C., Zimmermann, M., Biało, I., Martinelli, L., Fauqué, B., Choi, J., Garcia-Fernandez, M., Zhou, K.-J., Christensen, N.B., Kurosawa, T., Momono, N., Oda, M., Natterer, F.D., Fischer, M.H., Neupert, T., Chang, J.: Weak signal extraction enabled by deep neural network denoising of diffraction data. *Nature Machine Intelligence* **6**(2), 180–186 (2024) <https://doi.org/10.1038/s42256-024-00790-1>
- [22] Carbone, M.R., Topsakal, M., Lu, D., Yoo, S.: Machine-learning x-ray absorption spectra to quantitative accuracy. *Phys. Rev. Lett.* **124**, 156401 (2020) <https://doi.org/10.1103/PhysRevLett.124.156401>
- [23] Xian, R.P., Stimper, V., Zacharias, M., Dendzik, M., Dong, S., Beaulieu, S., Schölkopf, B., Wolf, M., Rettig, L., Carbogno, C., Bauer, S., Ernstorfer, R.: A machine learning route between band mapping and band structure. *Nature Computational Science* **3**(1), 101–114 (2023) <https://doi.org/10.1038/s43588-022-00382-2>
- [24] Chen, X., Sun, Y., Hruska, E., Dixit, V., Yang, J., He, Y., Wang, Y., Liu, F.: Detecting thermodynamic phase transition via explainable machine learning of photoemission spectroscopy. *Newton* **1**, 100066 (2025) <https://doi.org/10.1016/j.newton.2025.100066>
- [25] Kim, Y., Oh, D., Huh, S., Song, D., Jeong, S., Kwon, J., Kim, M., Kim, D., Ryu, H., Jung, J., Kyung, W., Sohn, B., Lee, S., Hyun, J., Lee, Y., Kim, Y., Kim, C.: Deep learning-based statistical noise reduction for multidimensional spectral data. *Review of Scientific Instruments* **92**(7), 073901 (2021)

<https://doi.org/10.1063/5.0054920>

- [26] Medarde, M.: Structural, magnetic and electronic properties of $R\text{NiO}_3$ perovskites (R =rare earth). *J. Phys. Condens. Matter* **9**, 1679 (1997)
- [27] Torrance, J.B., Lacorre, P., Nazzari, A.I., Ansaldo, E.J., Niedermayer, C.: Systematic study of insulator-metal transitions in perovskites $R\text{NiO}_3$ (R =Pr,Nd,Sm,Eu) due to closing of charge-transfer gap. *Phys. Rev. B* **45**, 8209 (1992)
- [28] Catalano, S., Gibert, M., Fowlie, J., Iniguez, J., Triscone, J.M., Kreisel, J.: Rare-earth nickelates $R\text{NiO}_3$: thin films and heterostructures. *Rep. Prog. Phys.* **81**, 046501 (2018)
- [29] Middey, S., Chakhalian, J., Mahadevan, P., Freeland, J.W., Millis, A.J., Sarma, D.D.: Physics of ultrathin films and heterostructures of rare-earth nickelates. *Annu. Rev. Mater. Res.* **46**, 305 (2016)
- [30] Chakhalian, J., Freeland, J.W., Millis, A.J., Panagopoulos, C., Rondinelli, J.M.: Colloquium: Emergent properties in plane view: Strong correlations at oxide interfaces. *Rev. Mod. Phys.* **86**, 1189 (2014)
- [31] Zhong, Y., Lee, K., Bhatta, R., Zhang, Y., Lee, Y., Gonzalez, M., Li, J., Wang, R., Hashimoto, M., Lu, D., Mo, S.-K., Jia, C., Hwang, H., Shen, Z.-X.: Surface preparation method for investigating the three-dimensional electronic structure of perovskite nickelates. *Phys. Rev. B* **112**, 035160 (2025) <https://doi.org/10.1103/wcm1-rrc5>
- [32] Lee, S., Chen, R., Balents, L.: Metal-insulator transition in a two-band model for the perovskite nickelates. *Phys. Rev. B* **84**, 165119 (2011) <https://doi.org/10.1103/PhysRevB.84.165119>
- [33] Chitturi, S.R., Ji, Z., Petsch, A.N., Peng, C., Chen, Z., Plumley, R., Dunne, M., Mardanya, S., Chowdhury, S., Chen, H., Bansil, A., Feiguin, A., Kolesnikov, A.I., Prabhakaran, D., Hayden, S.M., Ratner, D., Jia, C., Nashed, Y., Turner, J.J.: Capturing dynamical correlations using implicit neural representations. *Nature Communications* **14**(1), 5852 (2023) <https://doi.org/10.1038/s41467-023-41378-4>
- [34] Sitzmann, V., Martel, J.N.P., Bergman, A.W., Lindell, D.B., Wetzstein, G.: Implicit Neural Representations with Periodic Activation Functions (2020). <https://arxiv.org/abs/2006.09661>
- [35] Kingma, D.P., Ba, J.: Adam: A Method for Stochastic Optimization (2017). <https://arxiv.org/abs/1412.6980>
- [36] Meevasana, W., Zhou, X.J., Sahrakorpi, S., Lee, W.S., Yang, W.L., Tanaka, K., *et al.*: Hierarchy of multiple many-body interaction scales in high-temperature superconductors. *Phys. Rev. B* **75**, 174506 (2007)
- [37] Moritz, B., Schmitt, F., Meevasana, W., Johnston, S., Motoyama, E.M., Greven, M., Lu, D.H., Kim, C., Scalettar, R.T., Shen, Z.X., Devereaux, T.P.: Effect of strong correlations on the high energy anomaly in hole- and electron-doped high- T_C superconductors. *New J. Phys.* **11**, 093020 (2009)
- [38] Millis, A.J.: Lattice effects in magnetoresistive manganese perovskites. *Nature* **392**, 147–150 (1998) <https://doi.org/10.1038/32348>